



1 **Catchment-scale groundwater recharge and vegetation water use efficiency**

2

3 Peter A. Troch, Ravindra Dwivedi, Tao Liu, Antonio Alves Meira Neto, Tirthankar

4 Roy, Rodrigo Valdés-Pineda and Matej Durcik

5

6 *Department of Hydrology and Atmospheric Sciences, The University of Arizona*

7 *Tucson, AZ 85721, USA*

8 Saul Arciniega-Esparza and José Agustín Breña-Naranjo

9

10 *Instituto de Ingeniería, Universidad Nacional Autónoma de México, Mexico*

11

12 Key Points:

- 13 • An index of vegetation water use efficiency at the catchment scale (Horton
- 14 index) is a reliable predictor of long-term average recharge
- 15 • The Horton Index can be estimated using climate and catchment properties,
- 16 such as its aridity index, elevation and slope
- 17 • Average recharge rates at the catchment scale can be estimated without the
- 18 need for streamflow or groundwater observations

19



20

Abstract

21

22 Precipitation undergoes a two-step partitioning when it falls on the land surface. At
23 the land surface and in the shallow subsurface, rainfall or snowmelt can either
24 runoff as infiltration/saturation excess or quick subsurface flow. The rest will be
25 stored temporarily in the root zone. From the root zone, water can leave the
26 catchment as evapotranspiration or percolate further and recharge deep storage. It
27 was recently shown that an index of vegetation water use efficiency, the Horton
28 index (HI), could predict deep storage dynamics. Here we test this finding using 247
29 MOPEX catchments across the conterminous US. Our results show that the observed
30 HI is indeed a reliable predictor of deep storage dynamics. We also find that the HI
31 can reliably predict the long-term average recharge rate. Our results compare
32 favorably with estimates of average recharge rates from the US Geological Survey.
33 Previous research has shown that HI can be estimated based on aridity index, mean
34 slope and mean elevation of a catchment (Voepel et al., 2011). We recalibrated
35 Voepel's model and used it to predict the HI for our catchments. We then used these
36 predicted values of the HI to estimate average recharge rates for our catchments,
37 and compared them with those estimated from observed HI. We find that the
38 accuracies of our predictions based on observed and predicted HI are similar. This
39 provides a novel estimation method of catchment-scale long-term average recharge
40 rates based on simple catchment characteristics, such as climate and topography,
41 and free of discharge measurements.

42



43

44 Keywords: Horton Index, Total Storage, Deep Storage, Average Recharge, Water Use

45 Efficiency

46



47 **1. Introduction**

48 Soils, vegetation, and landforms at catchment scales have coevolved with climate,
49 geology and tectonics (*Troch et al.*, 2015) and these internal and external catchment
50 properties define the short- and long-term water balance components. Although the
51 role that climate (*Budyko*, 1974), climate seasonality (*Milly*, 1994; *Gentine et al.*,
52 2012), vegetation (*Zhang et al.*, 2001; *Williams et al.*, 2012; *Zhang et al.*, 2016;
53 *Donohue et al.*, 2012; *Donohue et al.*, 2007), soil characteristics (*Porporato et al.*,
54 2004; *Crosbie et al.*, 2010) and landscape features (*Shao et al.*, 2012; *Scanlon et al.*,
55 2006) exert on the long-term water balance components have been thoroughly
56 elucidated, the first-order controls of the inter-annual and inter-catchment
57 variability of water balance remain less understood.

58

59 Beyond Budyko's steady-state framework, several studies have investigated the role
60 of climate, vegetation and other catchment properties in hydrological partitioning
61 (*Farmer et al.*, 2003; *Troch et al.* 2009; *Voepel et al.*, 2011; *Arciniega-Esparza et al.*,
62 2016). For instance, *Farmer et al.* [2003] followed a top-down modeling approach to
63 study the differences in water balance of a range of semi-arid and temperate
64 catchments in Australia as a result of climate and landscape interactions. Their
65 results showed that process sensitivity changes with time scale, where drier
66 catchments are more sensitive to small time-scale perturbations. *Troch et al.* [2009]
67 studied the role of vegetation on hydrological partitioning through catchment-scale
68 water balance. They proposed the Horton Index (HI) as the ratio of catchment
69 vaporization and wetting (*Horton*, 1933). Applying the HI (see Equation 1) across



70 different ecosystems and spatial scales, they found that the water use efficiency of
71 vegetation increases in water-limited conditions. They further showed that the
72 adaptation of vegetation to climate change is similar across different ecosystem
73 types, this is, ecosystems tend to use water more efficiently as water availability
74 declines. *Voepel et al.* [2011] studied catchments from different ecoregions in the
75 USA and found that, in addition to the Aridity Index (ratio of annual potential
76 evaporation to precipitation), the HI is also dependent on mean catchment slope
77 and elevation, which means that the HI is related to (and hence can be predicted
78 from) the catchment characteristics controlling water retention in the catchment.
79 Unlike *Troch et al.* [2009] work, where catchment-scale vegetation water use
80 efficiency was solely derived using discharge measurements, *Voepel et al.* [2011]
81 successfully managed to test statistical regression predictors with the potential to
82 be further applied in ungauged catchments. More recently, *Arciniega-Esparza et al.*
83 (2016) investigated the dynamics between maximum total and deep catchment
84 storage and their relationship to vegetation water use efficiency as represented by
85 the HI in 33 semi-arid (water-limited) catchments in Mexico. They found that this
86 simple index of vegetation water use efficiency is a reliable predictor of deep
87 storage dynamics, where catchments with highly water-use efficient ecosystems
88 tend to generate lower amounts of baseflow that sustain riparian vegetation.
89 Furthermore, the HI could also explain how vegetation water use affects flow
90 persistence (perennial or ephemeral), as quantified by flow duration curves. These
91 findings suggested that catchment deep storage is both a cause and consequence of
92 vegetation dynamics and plant water use efficiency. Note that in our definition and



93 subsequent use of the HI term, we considered vegetation water use as synonymous
94 to catchment vaporization (V). The latter is usually justified, since the terrestrial
95 water loss is dominated by transpiration water loss [see i.e. *Jasechko et al.*, 2013;
96 *Maxwell and Condon*, 2016], even in semi-arid environments (Huxman et al., 2004).

97

98 The Horton Index is defined as:

$$99 \quad HI = \frac{V}{W} = \frac{P - Q_T}{P - Q_d} \quad (1)$$

100 where, V is vaporization (or ET, an estimate of vegetation water use), W is the
101 catchment wetting (or precipitation retained by the catchment), P is the
102 precipitation, Q_T is the total streamflow, and Q_d is direct or quick runoff. If we
103 hypothesize that HI is a reliable predictor of deep storage dynamics, or specifically
104 of long-term average recharge rates (R), Equation (1) can be used to state three
105 general assumptions about the relationship between HI and R . (1) When the
106 vaporization term is zero ($HI = 0$), it means that the vegetation is not using water;
107 therefore we assume that any source of precipitation would maximize the recharge
108 rates (R_{\max}), and would replenish deep storage. (2) If the vaporization equals the
109 wetting term ($HI=1$), we assume that all of the water retained in the catchment is
110 used by the vegetation; therefore the recharge rates would be zero, and deep
111 storage would not be able to sustain streamflow during dry periods. (3) We also
112 assume that the vegetation cannot consume more water than the one retained in the
113 catchment ($V \leq W$), therefore HI cannot have values larger than one. Under these
114 three assumptions we can expect that smaller values of HI (closer to zero) are



115 related to larger long-term average recharge rates. On the other hand, larger values
116 of HI (closer to one) are related to lower long-term average recharge rates. Figure 1
117 illustrates the different components of the annual water balance that define the
118 Horton index, and the three assumptions stated above.

119

120 The ability of HI to predict deep storage dynamics in other climatic regions and
121 varied geological settings has not been tested yet. In this study, we extend the
122 analysis of *Arciniega-Esparza et al. (2016)* to 247 MOPEX catchments located across
123 the conterminous US. Additionally, since the quantification of recharge rates at the
124 catchment scale is a challenging task and no reliable direct measurements exist, we
125 investigate whether the HI can be used to predict average baseflow conditions and
126 long-term average recharge rates at catchment scales. Assuming that the effective
127 recharge ultimately discharges to a stream and that baseflow consists entirely of
128 groundwater discharge, baseflow can provide a good approximation to recharge
129 (*Healy, 2010*).

130

131 Since it was shown that the HI can be predicted based on the aridity index, mean
132 slope and mean elevation of a catchment (*Voepel et al., 2011*), we further test
133 whether predicted HI values can reliably estimate average recharge rates for our
134 catchments. This is of utmost relevance for catchment hydrology as it goes a step
135 further in providing a connection between groundwater recharge, aquifer discharge
136 to streams during dry periods, streamflow regime type, and vegetation water-use
137 efficiency. In order to accomplish this, we employ bootstrapping to quantify the



138 sensitivity, robustness and reliability of HI-based deep storage predictions. Finally,
139 we compared our estimates of average annual groundwater recharge rates to a
140 recharge map for the conterminous US (*Wolock*, 2003).

141

142 **2. Data and Methods**

143 ***2.1 Study catchments and hydrological data***

144 For this study, 247 catchments were selected from the MOPEX (Model
145 Parameterization Estimation Experiment) database available at:
146 http://www.nws.noaa.gov/ohd/mopex/mo_datasets.htm (*Schaake et al.*, 2006).

147 These catchments span a wide range of climate and geomorphological settings
148 (Figure 2), and were selected because there were no missing records of daily
149 precipitation (P), discharge (Q), and potential evapotranspiration (PET) for our
150 period of analysis (1980-2002). We avoided missing data in order to exclude
151 misinterpretation of results due to data gap filling. We used the North American
152 Regional Reanalysis (NARR; *Mesinger et al.*, 2006) database to estimate actual
153 evapotranspiration for our selected catchments. The original dataset is provided in
154 3-hourly time steps with 32 km spatial resolution grid. We resampled the spatially
155 distributed actual evapotranspiration (AET) data to 6 km spatial scale and averaged
156 in space across the catchment areas and aggregated in time to obtain daily time
157 series. The nearest neighbor method was used to resample NARR data. This resampled
158 NARR dataset has been previously used by other studies (NARR; *Mesinger et al.*, 2006;
159 *Durcik et al.*, 2009). Please note that in general, resampling is not necessary to compute
160 spatially averaged AET values for the MOPEX basins; however, the resampling



161 improved the spatial representation of the grid cells, especially along the boundaries of
162 the catchments. We finally matched all the datasets and selected 23 hydrologic
163 (water) years (1980-2002) with complete records of P, Q, PET, and AET data. In this
164 study, a water year is defined as the period between October 1st and September 30th.
165 Our catchment dataset further includes catchment's landscape properties such as
166 drainage area, mean slope, mean elevation, and mean aspect calculated using the 3
167 arc-second (~90m) Shuttle Radar Topography Mission (SRTM) data (*Farr et al.*,
168 2007).

169

170 ***2.2 Estimation of Total and Deep Storage Dynamics***

171 For the purpose of our analysis, we define catchment total storage within a given
172 hydrologic year as derived from the time integration of the daily water balance
173 relative to some arbitrary initial value (zero total storage). Further, we define
174 catchment deep storage as the storage related to baseflow magnitudes, assuming
175 linear reservoir dynamics with a given reservoir constant. Table 1 summarizes the
176 nomenclature regarding different values and statistics of total and deep storage
177 used throughout the rest of this paper.

178

179 We used the same method as *Arciniega-Esparza et al.* (2016) to estimate total and
180 deep storage dynamics and statistics, and we summarize these methods here for
181 consistency. Total storage change was estimated using the daily water balance:

$$182 \quad \frac{dS_T}{dt} = P - ET - Q \quad (2)$$



183 where S_T is total storage relative to some arbitrary value, P is daily precipitation, E is
184 daily evapotranspiration and Q is daily discharge. Equation (2) was integrated every
185 hydrologic year, starting at October 1st assuming zero total storage. We corrected
186 the annual ET time series using the water balance method to ensure that the total
187 change of storage for any hydrologic year is zero. The correction was performed
188 proportional to the daily values of the initial ET data. We also tested whether
189 uncorrected ET values led to different result. We refer to the Discussion section for
190 more details. From the time series of S_T we then selected the maximum value to
191 represent that year's annual maximum total storage (Figure 3). We denote this
192 annual maximum total storage for a given year and a given catchment as S_T^{\max} (Table
193 1). For each catchment we obtained 23 annual maximum values of total storage, and
194 the average maximum total storage, \bar{S}_T^{\max} , was computed. This statistic was also used
195 by *Sayama et al.* (2011) to compare average maximum total storage to catchment
196 properties, such as average slope.

197

198 To estimate deep storage statistics, we performed streamflow separation and
199 baseflow recession analysis (*Tallaksen*, 1995; *Wittenberg and Sivapalan*, 1999;
200 *Sayama et al.*, 2011; *Arciniega-Esparza et al.*, 2016). Streamflow was partitioned into
201 quick flow (Q_d) and baseflow (Q_b) components using a recursive low-pass filter
202 (*Lyne and Hollick*, 1979). The one-parameter low-pass filter was passed three times
203 over the time series, two times forward and one time backward, to smoothen the
204 baseflow hydrograph (*Voepel et al.*, 2011). We selected a parameter value of 0.925
205 for all catchments, which is similar to the approach used in previous studies [*Voepel*



206 *et al.*, 2011; Arciniega-Esparza *et al.* 2016;]. This method has proven to be an
 207 effective tool to investigate the characteristics of storage feeding streams (Brutsaert,
 208 2008; Rupp and Woods, 2008; Sayama *et al.*, 2011). Once the annual baseflow
 209 hydrograph was obtained, we performed baseflow recession analysis, assuming that
 210 the deep storage dynamics can be represented by means of a linear reservoir:

$$211 \quad \frac{dS_D}{dt} = -Q_b = -\frac{S_D}{K} \quad (3)$$

212 where S_D is deep storage, Q_b is baseflow, and K is the linear reservoir constant.

213 Equation (3) can be rewritten as:

$$214 \quad -\frac{dQ_b}{dt} = \frac{1}{K} Q_b \quad (4)$$

215 Let $-dQ_b/dt=Y$ and $Q_b=X$. Equation (4) in terms of new variables X and Y is:

$$216 \quad Y = (1/K)X \quad (5)$$

217 Transforming Equation (5) in terms of square error (e_i) for $i=1,2,\dots,N$, where N = total
 218 number of days when $-dQ_b/dt$ or Y is positive, leads to the following equation:

$$219 \quad e_i^2 = (Y_i - \frac{1}{K} X_i)^2 \quad (6)$$

220 An optimization of Equation (6) with respect to the variable $1/K$ leads to the
 221 following Equation:

$$222 \quad \frac{d \sum_{i=1}^N e_i^2}{d(\frac{1}{K})} = 0 = -2 \sum_{i=1}^N X_i (Y_i - \frac{1}{K} X_i) \quad (7)$$

223 Thus, the value of the reservoir constant K for which Equation (6) represents a local
 224 minimum is:

$$225 \quad K = \frac{\sum_{i=1}^N X_i^2}{\sum_{i=1}^N X_i Y_i} = \frac{\sum_{i=1}^N Q_{b,i}^2}{\sum_{i=1}^N Q_{b,i} (-\frac{dQ_b}{dt})_i} \quad (8)$$

226



227 Equation (8) was used for estimating K for each hydrologic year and for each
228 catchment. Annual maximum deep storage (S_D^{\max}) was then computed using the
229 maximum baseflow value for each year (see Figure 3 for an illustration of our
230 method), multiplied by the K value from the same year. The 23 annual maximum
231 deep storage values obtained for each catchment were averaged to obtain the
232 average maximum deep storage, \bar{S}_D^{\max} , of the catchments.

233

234 ***2.3 Predictive relationships of storage dynamics and groundwater recharge***

235 Since total and deep storage are estimated using independent methods, the strength
236 of their relationship was analyzed to determine common patterns of inter-annual
237 and inter-catchment variability of storage dynamics. Several catchment
238 geomorphological properties (i.e. mean slope, drainage area, mean elevation, and
239 mean aspect, among others) were explored to predict storage dynamics. We also
240 explored the relationships with catchment vaporization (V), catchment wetting (W),
241 and the Horton Index, respectively. We further examined whether the HI can predict
242 certain statistics of the flow duration curve (FDC). We selected the 50th percentile
243 flow as a surrogate for average baseflow conditions. We tested whether the 50th
244 percentile represents accurately the observed average recharge rates for the
245 catchments. We also tested whether other streamflow percentiles would better
246 represent average baseflow conditions (see Discussion section for more details).
247 The advantage of using the FDC is that one does not have to perform hydrograph
248 separation to estimate average baseflow conditions and the average recharge rates
249 at catchment scale. As our MOPEX watershed dataset is composed of undisturbed



250 hydrological systems (*Schaake et al.*, 2006) and our analysis is based on 23
251 hydrologic years of climate data, aquifer storage tends to remain constant over the
252 long-term so that the steady-state hypothesis is valid (see Discussion in *Donohue et*
253 *al.*, 2007). In such cases, the difference between average baseflow conditions and
254 actual average recharge may be within the range of measurement uncertainty for
255 baseflow (*Healy*, 2010). A summary of our research structure is presented in Figure
256 4.

257

258 ***2.4 Independent estimation of average groundwater recharge rates***

259 It was previously shown that the HI can be reliably predicted based on the
260 catchment's aridity index, mean slope and mean elevation (*Voepel et al.*, 2011). We
261 tested whether predicted HI values can accurately estimate average recharge rates,
262 and how these predictions compare to those based on observed HI values. For this
263 purpose, we recalibrated Voepel's model, as that study used a different subset of
264 MOPEX catchments.

265

266 ***2.5 Quantifying sensitivity, robustness and reliability of predictive relationships***

267 We performed an uncertainty analysis using the Bootstrapping method to answer the
268 following questions: How much of the variance in the relationship between \bar{S}_D^{\max} and HI
269 can be explained by a linear fit between the two variables as a function of the number of
270 catchments used in the analysis (sensitivity)? How does the slope and intercept of the
271 linear fit between \bar{S}_D^{\max} and HI vary as a function of sample size (robustness)? How much
272 does the estimation error vary with sample size (reliability)? For answering the first two



273 questions, we randomly selected 1000 samples with replacement excluding x% of 247
274 catchments (called cutoff % here) and performed linear regression analysis to compare
275 explained variance and the values of the slope and the intercept of the linear regression
276 line for different cutoff levels. For performing the latter reliability analysis, we again
277 randomly selected 1000 samples with replacements excluding x% of 247 catchments and
278 performed a best-fit analysis for predicting the \bar{S}_D^{\max} vs. HI relationship. We then used the
279 predicted relationship to estimate \bar{S}_D^{\max} for the excluded x% catchments. Subsequently,
280 we computed the Mean Squared Error (MSE) at each of the cutoff % using the estimated
281 and known \bar{S}_D^{\max} values for those excluded x% catchments.

282

283 **3. Results**

284 ***3.1 Linear correlation between annual maximum total and deep storage***

285 The inter-annual linear correlation between the time series of annual maximum
286 total and annual maximum deep storage revealed that about 192 out of the 247
287 catchments show a positive correlation (Figure 5), and 55 catchments have negative
288 correlations. Of the 192 catchments with positive correlation between total and
289 deep storage, 96 catchments show a statistically significant correlation ($p < 0.05$),
290 and only one catchment of the 55 catchments with a negative correlation was
291 statistically significant. We removed the catchment that had a significantly negative
292 correlation between total and deep storage to avoid including a catchment that
293 possibly is affected by anthropogenic changes (e.g. pumping).

294

295 ***3.2 Predictors of average maximum total and deep storage***



296 *Inter-catchment variability*: Similar to previous findings regarding relationships
297 between catchment properties and storage dynamics (*Sayama et al., 2011; Voepel et*
298 *al., 2011; Arciniega-Esparza et al., 2016*), we too found that the mean catchment
299 slope is a strong control on average maximum total and average maximum deep
300 storage ($R=0.73$ and $R=0.69$, respectively). We also found that the inter-catchment
301 variability of total and deep storages is significantly correlated with mean
302 catchment wetting, and this relationship seems to be stronger than with catchment
303 slope (Figure 6, A1 and B1). On the other hand, vaporization does not seem to
304 correlate significantly with any of the storages (Figure 6, A2 and B2). Interestingly
305 and similar to *Arciniega-Esparza et al. (2016)*, deep storage dynamics are strongly
306 and significantly correlated with the mean HI, while the correlation between HI and
307 total storage is weaker than between wetting and total storage. It shouldn't be
308 surprising that the HI is related to the average maximum deep storage, as the latter
309 is related to the average baseflow. Since the empirical HI is derived from baseflow
310 separation, there is obviously a strong relationship with average baseflow. The
311 linear pattern shown in Figure 6 (B3) reveals the nature of the relationship between
312 empirical HI and average maximum deep storage, and indicates that HI can be an
313 candidate to predict deep storage dynamics at regional scales. The fact that HI
314 expresses catchment vegetation water use efficiency indicates the important role of
315 terrestrial vegetation in controlling deep groundwater percolation which sustains
316 baseflow conditions across a wide range of climates and geological settings (*Troch*
317 *et al., 2009*). It remains to be investigated whether predictions of the empirical HI



318 based on independent climate and catchment characteristics can be used to
319 estimate storage dynamics at regional scales (see Section 3.3.2).

320

321 *Inter-annual variability*: Figure 7 shows the correlation coefficients between storage
322 dynamics and water balance components (wetting, W , vaporization, V , and their
323 ratio, $HI=V/W$) based on annual values. Considering the coefficients of
324 determination (R^2 , not shown), the inter-annual variability of storage dynamics
325 compared to wetting, vaporization, and HI revealed that catchment wetting could
326 significantly explain inter-annual variability of total storage for 68% of the
327 catchments (Figure 7, A1). Catchment wetting inter-annual variability can also
328 explain inter-annual variability of deep storage of about 46% of the catchments
329 (Figure 7, B1). Catchment vaporization explained inter-annual variability of the total
330 and deep storages for 51% and 22% of the catchments, respectively. The inter-
331 annual variability of the HI could explain inter-annual variability of deep storage for
332 95% of the catchments (Figure 7, B3), but total storage inter-annual variability was
333 only explained for 27% of the catchments (Figure 7, A3). Again, it is not surprising
334 that the annual empirical HI is related to annual deep storage dynamics, and thus to
335 annual average baseflow. Figure 7-B3 simply reveals the nature of this relationship.

336

337 ***3.3 The Horton Index, streamflow persistence and average recharge rates***

338 *3.3.1 Observed HI based estimates*

339 We further investigated whether the observed HI is a good predictor for catchment-
340 scale groundwater recharge. We found that there is a clear pattern between the



341 catchment HI and the relative position of the flow duration curve (Figure 8). Low
342 values of HI correspond to sustained higher flow, i.e., perennial streams, whereas
343 high values of HI are related to much lower flows, i.e., ephemeral streams. We found
344 that for $HI=0.86$, catchments switch between perennial to ephemeral flow regimes.
345 The value of $HI=0.86$ was determined from the flow duration curves subject to the
346 condition that the lowest HI for which streamflow first approaches a zero value. We
347 call this the “Critical Horton Index”. Arciniega-Esparza et al. (2016) found the same
348 critical HI value for the semi-arid catchments in Mexico.

349

350 The relationship between mean baseflow derived from our baseflow separation
351 method (Q_b) and the 50th percentile (Q_{50}) of the catchment streamflow is strongly
352 significant ($R^2=0.96$; $p=0.00$) (Figure 9A). However, the slope of the relationship is
353 different from 1 (0.7), therefore predictions of average baseflow based on Q_{50} could
354 be overestimated. Q_{50} is only an efficient surrogate of average baseflow conditions
355 for the catchments under consideration if the slope of the regression line is one. In
356 the Discussion section, we address this limitation of the method. Nevertheless, we
357 found that the linear correlation between Q_{50} and HI is strongly significant ($p<0.05$),
358 and explains 72% of the variance (Figure 9B). These results suggest that under long-
359 term steady state conditions, recharge rates can be predicted using an index of
360 water use efficiency.

361

362 Our estimates of average recharge rates (using the results from Figure 9) compared
363 against the average recharge rates map from the USGS [*Wolock, 2003*], revealed a



364 strong similarity between their spatial variability (Figure 10). Moreover, the inter-
365 catchment variability revealed a significant positive correlation while comparing the
366 absolute values of average recharge rates from both sources (Figure 11). This
367 finding is encouraging as the recharge rates in both sources are calculated
368 differently. The USGS groundwater recharge estimates are derived from the
369 baseflow index - the ratio of base flow to total flow - map for the conterminous US
370 [Wolock, 2003], while ours is based on the Horton index.

371

372 3.3.2 Predicted HI based groundwater recharge estimations

373 The estimation of deep storage dynamics and hence average recharge rates based
374 on the HI is only useful if we are able to estimate the HI independently. Without
375 such independent estimates the method becomes circular: derive the HI from
376 baseflow separation to predict baseflow characteristics. Voepel *et al.* (2011) used a
377 multiple linear regression model to predict HI based on aridity index (AI), mean
378 slope (β) and mean elevation (Z). Since Voepel *et al.* (2011) used a different subset
379 of MOPEX catchments, we recalibrated his multiple regression model for our 246
380 catchments and found the best fit ($R^2=0.72$) using:

$$381 \quad HI=0.78+0.11 \ln(AI)-0.03 \beta-0.04Z \quad (9)$$

382 Note that β is fractional slope and $\ln(AI)$, β and Z are normalized variables using
383 mean and standard deviations of the observed values for the 246 MOPEX
384 catchments. For normalization of $\ln(AI)$, β and Z , the following values were used: (i)
385 mean and standard deviation of $\ln(AI)$ is -0.06 and 0.45, resp.; (ii) mean and
386 standard deviation of β (fractional) is 0.06 and 0.05, resp.; (iii) mean and standard



387 deviation of Z (m) is 631.73 m amsl and 613.68 m amsl, resp. Figure 12 shows the
388 comparison between observed and predicted HI based on Equation 9. The best linear fit
389 corresponded to a coefficient of determination R^2 of 0.78.

390

391 As shown in Figure 13, estimates of catchment-scale groundwater recharge based
392 on predicted HI values are very similar to those based on observed HI values. We
393 thus have now a method that can estimate regional recharge rates based on easily
394 obtainable catchment characteristics, such as climate and topography.

395

396 ***3.4 Reliability of estimation methods***

397 In order to test the reliability of the methods developed, we performed a
398 bootstrapping analysis to examine the effect of sample size on model performance.
399 First, we investigated how the explained variance of our average recharge rate
400 model changes with sample size (Figure A1). As we systematically decrease the
401 number of catchments in our sample, we observe that the range of coefficients of
402 determination increases symmetrically around a very constant mean. Even with
403 95% of the catchments removed from model fitting, the model can, on average,
404 explain the same amount of variance as the model based on all 246 catchments.
405 With 50% of the catchments removed, we see that the range of explained variance is
406 between 0.7 and 0.9, a relatively narrow range.

407

408 Next, we looked at the robustness of the linear regression model in terms of slope
409 and intercept value (Figure A2 and A3). Again, we observe that on average the slope



410 and intercept values of the linear regression models are very stable, and that the
411 uncertainty about the mean values grows symmetrically about the mean with
412 decreasing sample size.

413

414 Finally, the reliability of the linear regression model was tested (Figure A4). After
415 removing $x\%$ of catchments to fit a linear regression model and using the same
416 model to predict the average recharge rate for the remaining $x\%$ catchments, we see
417 that the MSE slightly increases. Moreover, removing 5% of all catchments results in
418 mean square errors (MSE) having a wide range, from very low MSE to very high
419 MSE. This is due to the fact that it is very likely that in 1000 runs, 5% 'good'
420 catchments are selected (catchments that fall on the regression line estimated by
421 the remaining 95%) but it is equally likely that 5% 'bad' catchments (catchments
422 that don't fall on the regression line) are also selected. As the number of catchments
423 left out of the analysis are increased, the probability of selecting all 'good' or all 'bad'
424 catchments decreases, and this is reflected in the reduced range of MSE values. Only
425 when leaving out 95% of the catchments, there is an increase in the range of MSE
426 values, because the remaining 5% catchments are likely to result in unreliable
427 regression models.

428

429 **4. Discussion**

430 The results presented in this paper confirm that average maximum total storage and
431 average maximum deep storage are positively correlated at a similar level (78%)
432 compared to a previous study (73%) performed across an arid region (Arciniega-



433 Esparza et al., 2016). Other similarities with *Arciniega-Esparza et al.* (2016) study
434 were found when examining the relationship between maximum catchment storage
435 and its mean catchment slope. In fact, the role of slope in total and deep storage was
436 more prominent for the MOPEX dataset ($R=0.73$ and $R=0.69$, respectively) than in
437 Mexico's drylands ($R=0.59$ and $R=0.52$), but very similar ($R=0.74$ only for maximum
438 storage) to a group of small watersheds in Northern California (*Sayama et al.*, 2011).
439 This suggests that in arid regions, catchment slope become less relevant to predict
440 its maximum storage capacity when compared to wetter regions.

441

442 Nevertheless, the variables that correlate strongest with deep storage dynamics
443 were catchment wetting ($R=0.70$) and the Horton Index ($R=-0.88$), respectively.
444 Surprisingly, the magnitude of the correlation between these variables and different
445 storages across the region of study is very similar and only ~10% of the catchments
446 seem to be out from these observed patterns.

447

448 In addition to the observed connection between deep storage and the HI, the HI
449 turns out to be a simple but reliable classification tool for streamflow persistence. A
450 threshold value (named the Critical Horton Index) that separates streams with
451 perennial regimes from intermittent and/or ephemeral flows was found similar as
452 in *Arciniega-Esparza et al.* (2016) study. This threshold determines the link between
453 vegetation water-use efficiency and the time that a minimum amount of
454 groundwater outflow ($Q>0$) to a stream is likely to occur. It suggests that
455 catchments must reach high vegetation water-use efficiency levels ($HI>0.86$) in



456 order to deplete the active catchment storage (storage that continuously interacts
457 with the stream network) during some time of the hydrologic year.

458

459 In addition to the assumptions mentioned in the introduction of this paper, there
460 are other important assumptions underlying the proposed method of using the
461 Horton index estimated from climate and landscape characteristics that can limit its
462 applicability. First, in order to interpret the Horton index as a vegetation water use
463 efficiency, as in Troch et al. (2009), we have to assume that transpiration is the main
464 component in catchment vaporization or evapotranspiration. This is generally the
465 case in vegetated landscapes, but will obviously not be the case in poorly vegetated
466 arid catchments. Therefore, the proposed method cannot be used to estimate
467 recharge rates in desert landscapes (except, perhaps, in the Sonoran Desert of the
468 SW USA, which has significant green cover throughout the rainy seasons).

469

470 Second, the low pass filter of *Lyne and Hollick* (1979) is a reasonable method to
471 separate quick runoff from baseflow. Without additional information about the
472 chemistry of streamflow and the different sources of streamflow (groundwater, soil
473 water and rainfall) there is no way to test the reliability of this baseflow separation
474 method. In this study, we have opted to use a single parameter that defines the cut-
475 off frequency of the low pass filter across all catchments, but if better information
476 about end-members' chemistry is available this parameter could possibly be
477 optimized for specific catchments.

478



479 Third, we assume that baseflow is equal to recharge, and that aquifer storage is
480 constant over the long term. This will only be true in catchments with unregulated
481 streamflow, without upstream extraction of surface and/or groundwater, without
482 lateral groundwater flow into and out of the catchment topographic divide, and
483 without significant evapotranspiration from the groundwater table. The MOPEX
484 catchments were selected to avoid such effects on streamflow, but since the
485 compilation of the database it is possible that some catchments have undergone
486 some type of anthropogenic impacts.

487

488 Finally, we assumed that long-term average baseflow conditions can be estimated
489 from the 50th percentile of the flow duration curve (Q_{50}). This choice was more an
490 intuitive guess than an informed decision. We tested this assumption for our
491 catchments and found that Q_{65} in fact is a much better estimate of average baseflow
492 conditions. For the selected catchments, there exists a one-to-one relationship
493 between Q_{65} and average baseflow, and both variables are highly correlated ($R^2 =$
494 0.90). Before we can replace Q_{50} with Q_{65} more research is required to check how
495 universal this finding is across different climates and geologies.

496

497 There can be a perceived possibility that some of the statistical relationships shown
498 in this study are the result of spurious correlation (i.e. The HI is estimated from
499 baseflow separation and is then used to estimate average baseflow conditions).
500 There are several arguments that go against this statement, but the strongest that
501 we can think of is the fact that we use predicted HI from climate and landscape



502 properties to estimate average baseflow and long-term recharge. The fact that the
503 HI is correlated with climate and landscape properties indicate that we can interpret
504 the HI as an index of catchment co-evolution of soils, vegetation and landforms with
505 climate and geology. It is therefore possible that the proposed method would only
506 work in catchments where vegetation is in equilibrium with the local climate. Non-
507 native species colonizing catchments could possibly off-set such equilibrium, and
508 therefore caution is warranted to apply the method when that is the case.

509

510 **5. Conclusions**

511 In this paper, three different recharge estimation methods were compared: (i) a
512 conventional method (*Wolock et al., 2003*) based on physical hydrology (annual
513 runoff and baseflow index), (ii) a methodology based on a catchment
514 ecohydrological index derived from observed discharge records (*Troch et al., 2009*),
515 and (iii) a methodology based on a predicted ecohydrological index using climate
516 and topography data (*Voepel et al., 2011*). Differences between groundwater
517 recharge estimates from the observed and predicted HI are minimal, suggesting that
518 both methods are good proxies for long-term average groundwater recharge. In this
519 work, we showed that the former can be widely used in gauged catchments while
520 the latter has the potential to be applied in ungauged catchments.

521

522 This synthesis study tested a parsimonious modeling framework based on the Horton
523 Index, a catchment index that combines in a simple way the effects of storage
524 capacity of soils (*Horton, 1933*), topography (*Voepel et al., 2011; Thompson et al.,*



525 2012), and ecosystems (*Troch et al., 2009; Huxman et al., 2004*) on hydrological
526 partitioning. It effectively expresses how much water, available to the catchment's
527 ecosystem, is being used by the plants. This water use efficiency metric increases
528 with climate aridity while its value becomes less in temperate and humid regions.
529 From our results we observe that when the HI crosses a critical value (0.86),
530 catchments' main streams become intermittent or ephemeral. The flow duration
531 curves of catchments rank quantitatively with HI (high to low flows corresponding
532 to low and high HI, respectively), suggesting that the statistical distribution of
533 streamflow regimes, including median flows (a proxy for recharge), is primarily
534 controlled by vegetation water use.

535

536 This work (based on a large hydrological sample) provides further evidence that: (a)
537 maximum total and deep catchment storage are mainly positively correlated and (b)
538 vegetation water-use efficiency (the Horton Index) is a robust predictor for low-
539 flows and groundwater recharge in catchments with different types of climate, soils,
540 geology and vegetation cover. Future work could explore the suitability of the
541 Horton Index for inferring low-flows and recharge at shorter timescales, analyze
542 long-term changes in climate, water-use efficiency and catchment storage, and
543 investigate the behavior of HI at smaller spatial scales (e.g. zero-order basins and
544 experimental plots/hillslopes), among others.

545

546

547 **6. Acknowledgements**



548 This work was greatly improved from comments made by three anonymous
549 reviewers. The authors acknowledge funding through a CAZMEX (UA-CONACYT)
550 research grant. Antonio Meira would like to acknowledge financial support from the
551 Brazilian Mobility Program, through the CAPES Foundation, Brazil. Rodrigo Valdés-
552 Pineda would like to acknowledge funding from the National Commission of Science
553 and Technology of Chile (CONICYT). The data used to produce this paper is available
554 upon request with Matej Durcik.
555



556 **7. References**

- 557 Arciniega-Esparza, S., Breña-Naranjo, J. A., and Troch, P. A., On the connection
558 between terrestrial and riparian vegetation: the role of storage partitioning in
559 water-limited catchments, *Hydrological Processes*, 10.1002/hyp.11071, 2016.
- 560 Brutsaert, W., Long-term groundwater storage trends estimated from streamflow
561 records: Climatic perspective. *Water Resources Research*, 44(2), 2008..
- 562 Budyko, M. I., *Climate and Life*, Int. Geophys. Ser., vol. 18, 508 pp., Academic, N. Y.,
563 1974
- 564 Crosbie, R. S., Jolly, I. D., Leaney, F. W., and Petheram C., Can the dataset of field based
565 recharge estimates in Australia be used to predict recharge in data-poor areas?,
566 *Hydrology and Earth System Sciences*, 14(10), 2023-2038, 2010
- 567 Donohue, R. J., Roderick, M. L., & McVicar, T. R., On the importance of including
568 vegetation dynamics in Budyko's hydrological model. *Hydrology and Earth System*
569 *Sciences*, 11, 983–995, 2007
- 570 Farmer, D., Sivapalan, M., & Jothityangkoon, C., Climate, soil, and vegetation controls
571 upon the variability of water balance in temperate and semiarid landscapes:
572 Downward approach to water balance analysis. *Water Resources Research*, 39(2),
573 2003.
- 574• Farr, T.G., Rosen, P.A., Caro, E., Crippen, R., Duren, R., Hensley, S., Kobrick, M., Paller,
575 M., Rodriguez, E., Roth, L., Seal, D., Shaffer, S., Shimada, J., Umland, J., Werner, M.,
576 Oskin, M., Burbank, D., Alsdorf, D., The shuttle radar topography mission, *Rev.*
577 *Geophys.*, 45, RG2004, doi:10.1029/2005RG000183, 2007.



- 578 Gentine, P., D'Odorico, P., Lintner, B. R., Sivandran, G., and Salvucci, G.,
579 Interdependence of climate, soil, and vegetation as constrained by the Budyko
580 curve, *Geophys. Res. Lett.*, 39, L19404, doi:10.1029/2012GL053492, 2012
- 581 Healy, R. W., *Estimating Groundwater Recharge*, Cambridge Univ. Press, Cambridge,
582 U. K., 2010
- 583 Horton, R. E., The role of infiltration in the hydrologic cycle. *Transactions of the*
584 *American Geophysical Union* 14: 446– 460, 1933.
- 585 Jasechko, S., Sharp, Z. D., Gibson, J. J., Birks, S. J., Yi, Y., and Fawcett, P. J., Terrestrial
586 water fluxes dominated by transpiration, *Nature*, 496(7445), 347-350, 2013.
- 587 Lyne, V. and Hollick, M., Stochastic time-variable rainfall runoff modeling, in
588 *Hydrology and Water Resources Symposium*, Natl. Comm. on Hydrol. and Water
589 *Resour. of the Inst. of Eng., Perth, Western Aust., Australia.*, 1979.
- 590 Maxwell, R. M., and Condon, L. E., Connections between groundwater flow and
591 Transpiration partitioning, *Science*, 353(6297), 377-380, 2016.
- 592 Milly, P., Climate, soil-water storage, and the average annual water-balance, *Water*
593 *Resour. Res.*, 30(7), 2143–2156, doi:10.1029/94WR00586, 1994.
- 594 Porporato, A., Daly, E., and Rodríguez-Iturbe, I., Soil water balance and ecosystem
595 response to climate change, *Am. Nat.*, 164(5), 625–632, doi:10.1086/424970,
596 2004.
- 597 Rupp, D. E., and Woods, R. A., Increased flexibility in base flow modelling using a
598 power law transmissivity profile. *Hydrological processes*, 22(14), 2667-2671,
599 2008.
- 600 Sayama, T., McDonnell, J. J., Dhakal, A., and Sullivan, K., How much water can a



- 601 watershed store?. *Hydrological Processes*, 25(25), 3899-3908, 2011.
- 602 Scanlon, B. R., Keese, K. E., Flint, A. L., Flint, L. E., Gaye, C. B., Edmunds, W. M., and
603 Simmers, I., Global synthesis of groundwater recharge in semiarid and arid regions,
604 *Hydrological Processes*, 20(15), 3335-3370, 2006.
- 605 Schaake, J., Cong, S., and Duan, Q., U.S. MOPEX DATA SET, NOAA National Weather
606 Service, Silver Spring, MD, 23 p., 2006.
- 607 Shao, Q., Traylen, A., and Zhang, L., Nonparametric method for estimating the effects
608 of climatic and catchment characteristics on mean annual evapotranspiration,
609 *Water Resour. Res.*, 48, W03517, doi:10.1029/2010WR009610, 2012.
- 610 Tallaksen, L. M., A review of baseflow recession analysis. *Journal of hydrology*,
611 165(1-4), 349-370, 1995.
- 612 Troch, P. A., Martinez, G. F., Pauwels, V. R. N., Durcik, M., Sivapalan, M., Harman, C.,
613 Brooks, P. D., Gupta, H. and Huxman, T., Climate and vegetation water use
614 efficiency at catchment scales, *Hydrol. Process.*, 23(16), 2409-2414,
615 doi:10.1002/hyp.7358, 2009.
- 616 Troch, P. A., Lahmers, T., Meira, A., Mukherjee, A., Pedersen, J. W., Roy, T., and
617 Valdes-Pineda, R., Catchment coevolution: A useful framework for improving
618 predictions of hydrological change?, *Water Resour. Res.*, 51,
619 doi:10.1002/2015WR017032, 2015.
- 620 Voepel, H., Ruddell, B., Schumer, R., Troch, P. A., Brooks, P. D., Neal, A., ... & Sivapalan,
621 M., Quantifying the role of climate and landscape characteristics on hydrologic
622 partitioning and vegetation response. *Water Resources Research*, 47(10), 2011.



623 Christopher A. W., Reichstein M., Buchmann N., Baldocchi D., Beer C., Schwalm C.,
624 Wohlfahrt G., Hasler N., Bernhofer C., Foken T., Papale D., Schymanski S., Schaefer K.,
625 Climate and vegetation controls on the surface water balance: Synthesis of
626 evapotranspiration measured across a global network of flux towers, *Water Resour.*
627 *Res.*, 48, W06523, doi:10.1029/2011WR011586, 2012.

628 Wittenberg, H., and Sivapalan, M., Watershed groundwater balance estimation using
629 streamflow recession analysis and baseflow separation. *Journal of hydrology*,
630 219(1), 20-33, 1999.

631 Wolock, D. M., Estimated mean annual natural ground-water recharge in the
632 conterminous United States, edited, U.S. Geological Survey, VA, 2003.

633 Zhang, L., Dawes, W. R., and Walker, G. R., Response of mean annual
634 evapotranspiration to vegetation changes at catchment scale. *Water resources*
635 *research*, 37(3), 701-708, 2001.

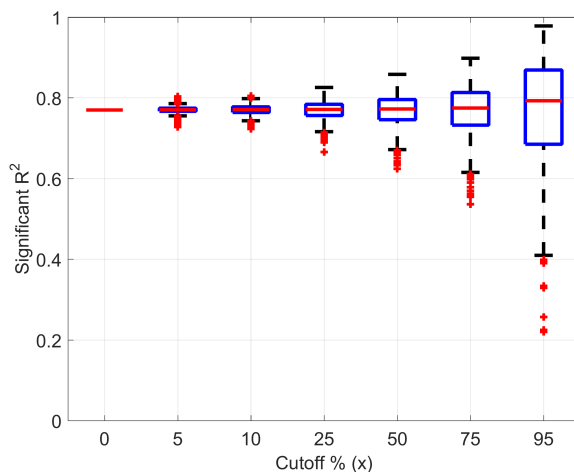
636 Zhang, S., Yang, H., Yang, D., & Jayawardena, A. W., Quantifying the effect of
637 vegetation change on the regional water balance within the Budyko framework.
638 *Geophysical Research Letters*, 43(3), 1140-1148, 2016.

639

640

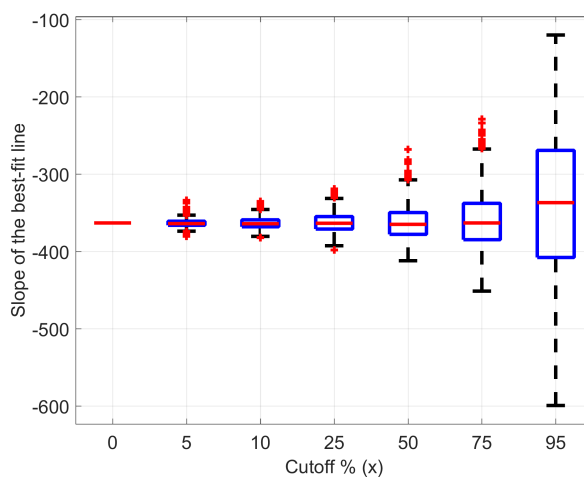


641 **Appendix A**



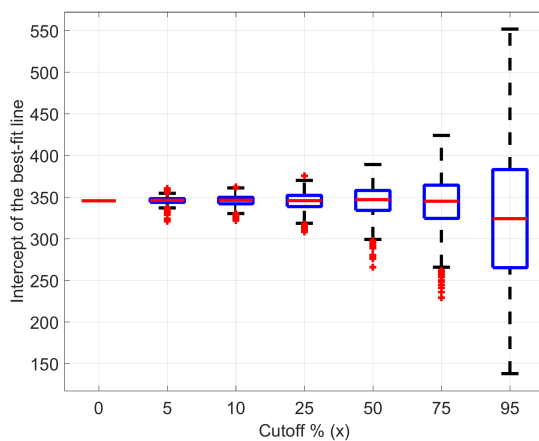
642

643 **Figure A1: Box-Whisker plots of explained variance (R^2 : coefficients of**
644 **determination) with increasing cutoff level**



645

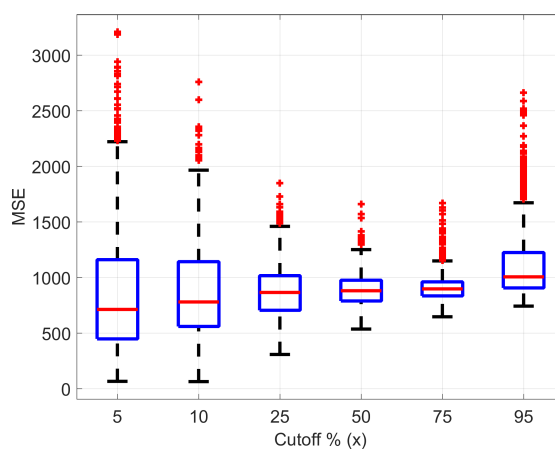
646 **Figure A2: Box-Whisker plots of slope of the linear regression model with increasing**
647 **cutoff level**



648

649 Figure A3: Box-Whisker plots of intercept of the linear regression model with

650 increasing cutoff level



651

652 Figure A4: Box-Whisker plots of the mean squared error (MSE) with increasing

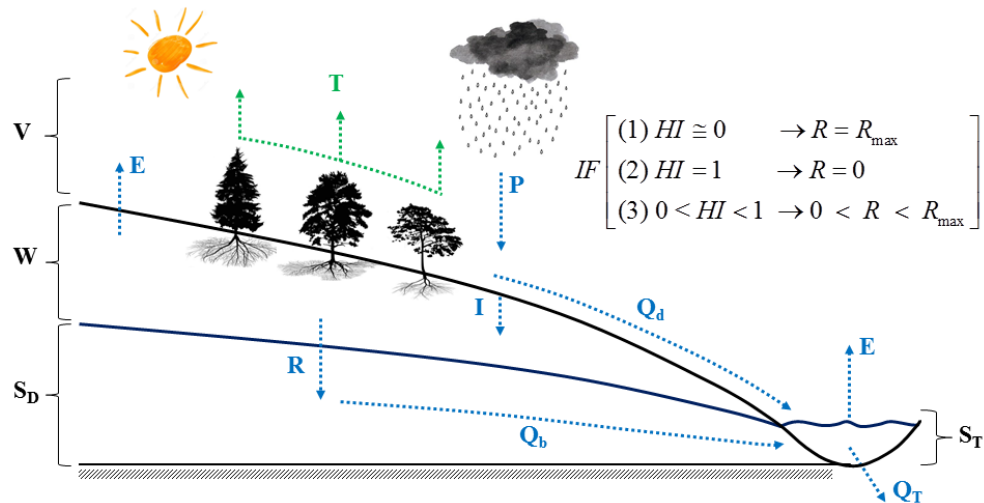
653 cutoff level

654



655 **Figures**

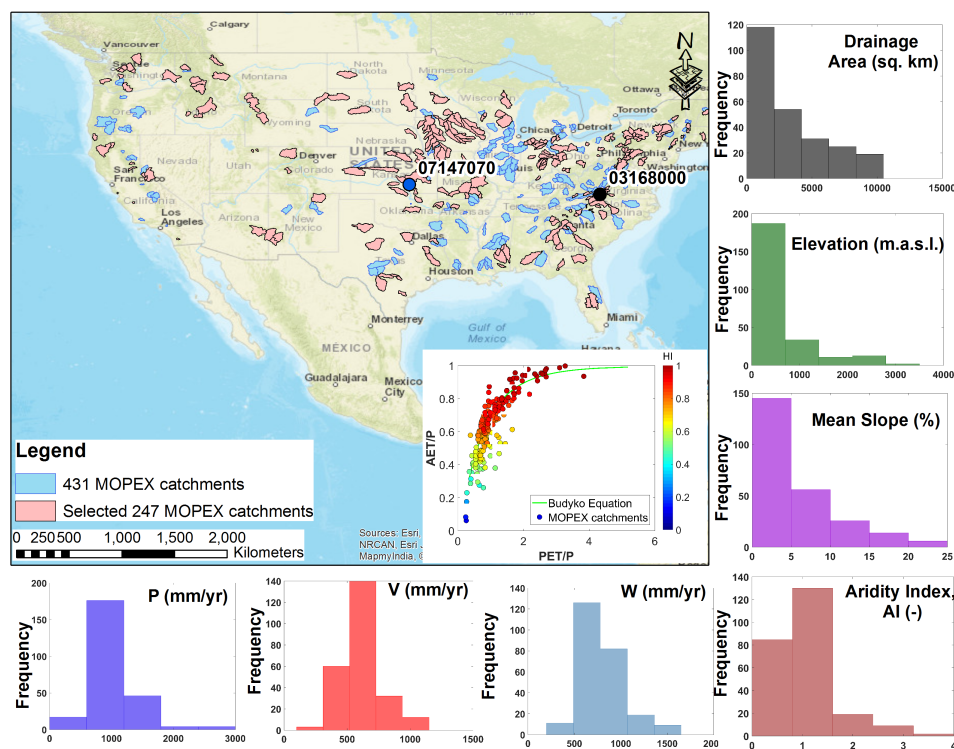
$$HI = \frac{V}{W} = \frac{P - Q_T}{P - Q_d} = \frac{P - (Q_d + Q_b)}{P - (Q_T - Q_b)} = \frac{P \text{ that does not become streamflow}}{P \text{ retained by the catchment}}$$



656

657 **Figure 1:** A conceptual-level representation of hydrological processes and annual
 658 water balance components that define the Horton index (HI). P is annual
 659 precipitation, E is annual evaporation, T is annual transpiration, I is annual
 660 infiltration, R is annual recharge, Q_d is annual quick or direct runoff, Q_b is annual
 661 baseflow, and Q_T is total annual streamflow. V is vaporization as the sum of E and T,
 662 W is wetting or annual infiltration, S_D is deep storage and S_T is total storage as
 663 derived from the catchment water balance. The three general assumptions
 664 underlying the relationship between HI and R are also displayed.

665



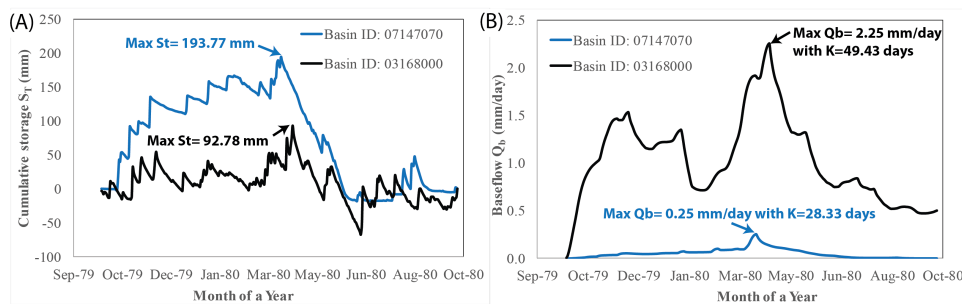
666

667 **Figure 2:** Study area and selected 247 catchments out of a total of 431 MOPEX
 668 catchments. The Budyko curve (color-coded using the catchments' Horton index)
 669 and the histograms of some catchment climate and landscape properties (i.e.
 670 precipitation (P), vaporization (V), wetting (W), aridity index, drainage area, slope,
 671 and elevation) are presented as insets. The two catchments for which the USGS
 672 stream gaging codes are provided in this plot correspond to the two catchments
 673 used in Figure 3.

674



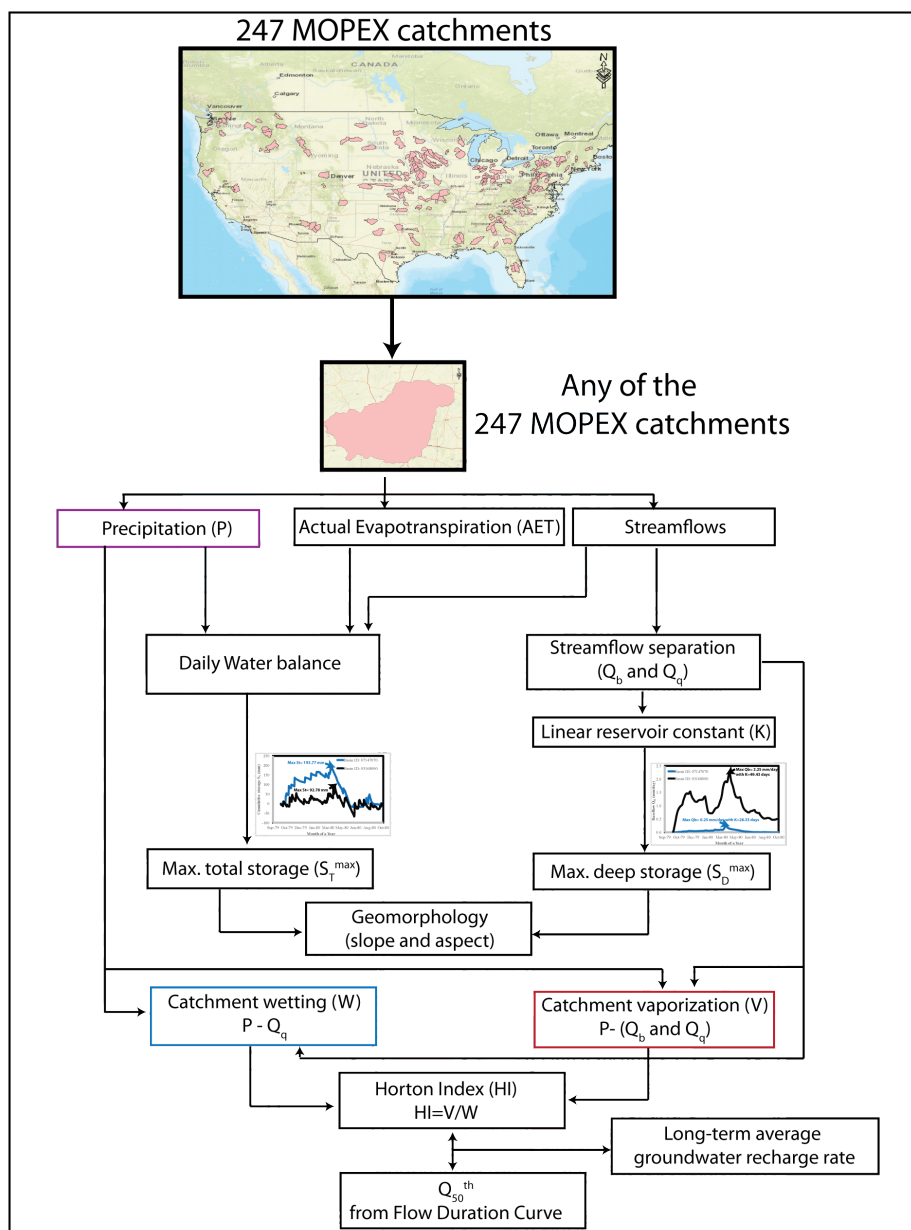
675



676

677 **Figure 3:** Examples of daily time series of total (S_T) and deep storage (S_D) for the
678 catchments highlighted in Figure 2. (A) Time series of S_T ; (B) Time series of S_D . The
679 locations of the two catchments shown in this figure are given in Figure 2.

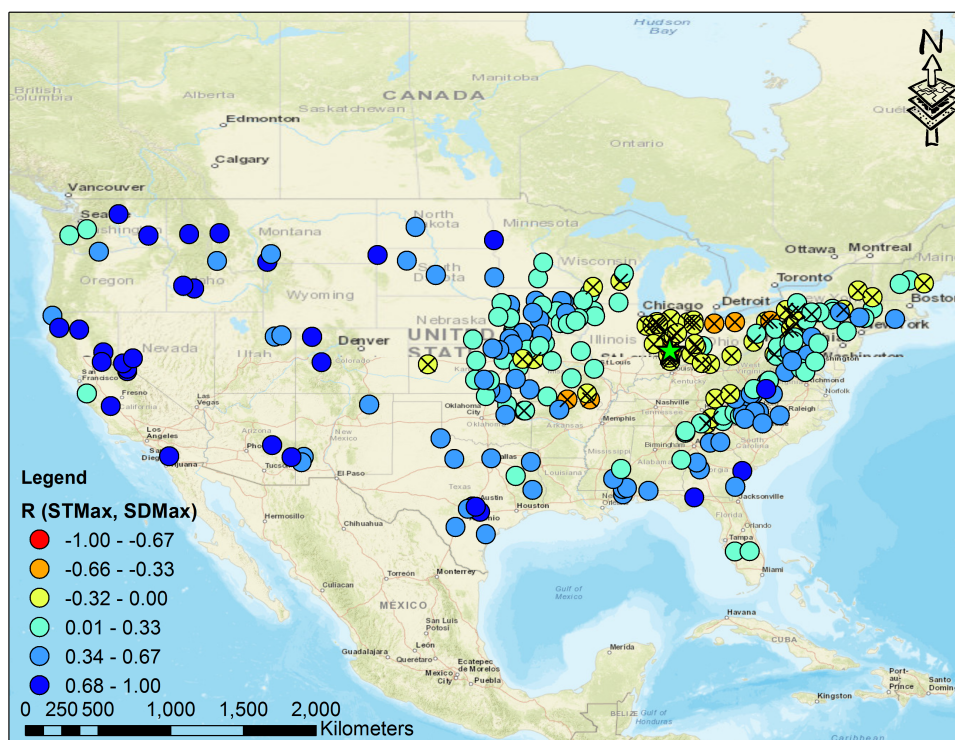
680



681

682 **Figure 4:** Research structure used to determine storage dynamics and potential

683 predictors of baseflow conditions and groundwater recharge.



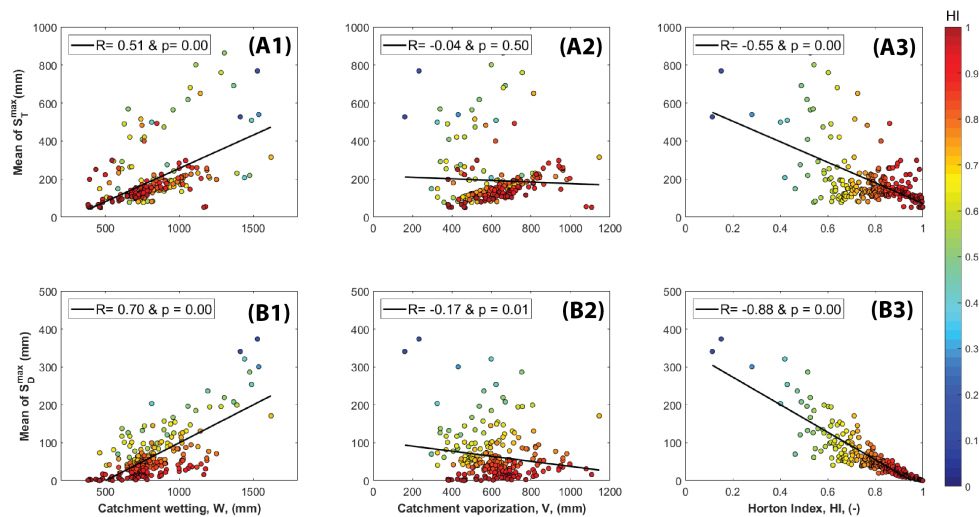
684

685 **Figure 5:** Correlation coefficients between annual maximum total (ST_{Max}) and
686 annual maximum deep storage (SD_{Max}) for 247 MOPEX catchments in the
687 conterminous US. Crossed markers show the catchments with a negative
688 relationship (55 catchments) between the two types of storage, but the relationship
689 is only significant for one catchment (shown by the green star).

690



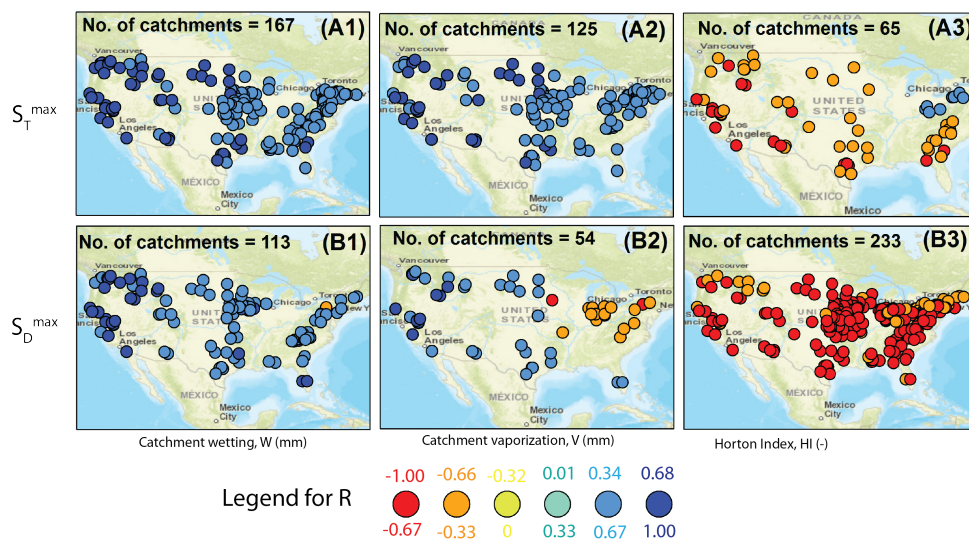
691

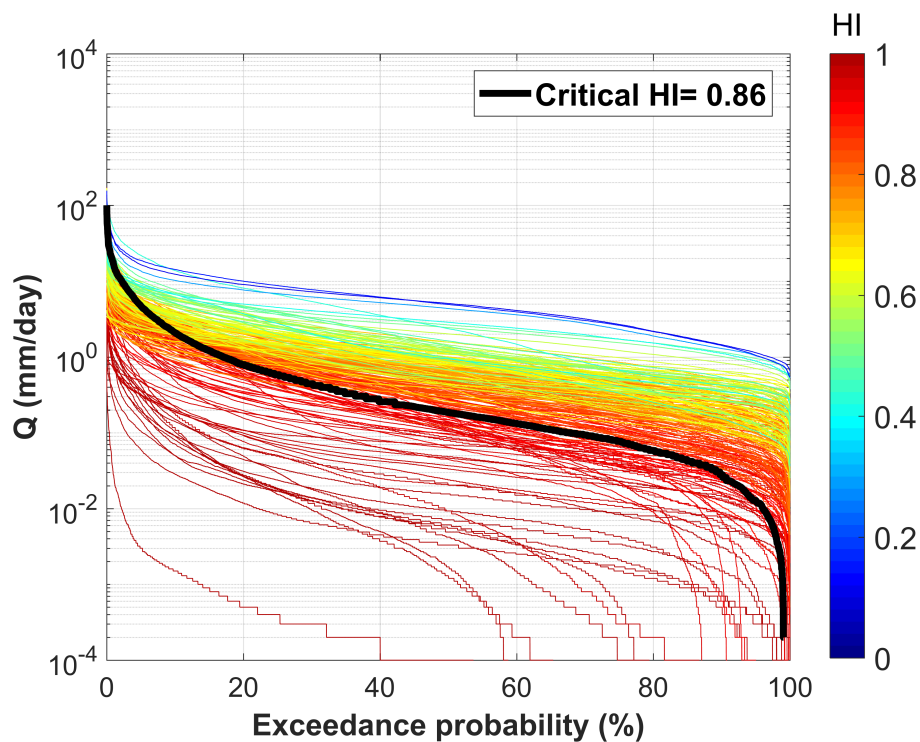


692

693 **Figure 6:** Linear relationships between average catchment wetting, vaporization,
694 and the Horton index versus (A) average maximum total storage and (B) average
695 maximum deep storage for the selected 246 MOPEX catchments.

696





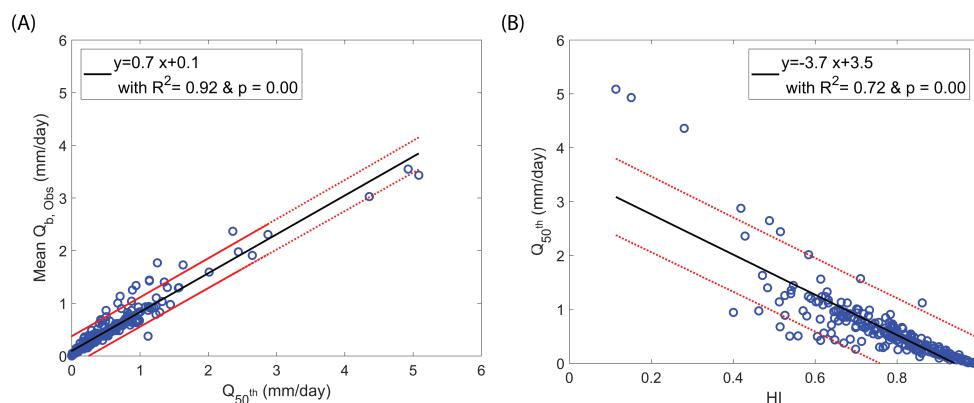
703

704 **Figure 8:** Flow duration curves for 247 MOPEX catchments under study. The color-
705 scheme is related to the catchment average Horton Index. The black line separates
706 perennial streams from ephemeral streams at the critical HI=0.86.

707



708



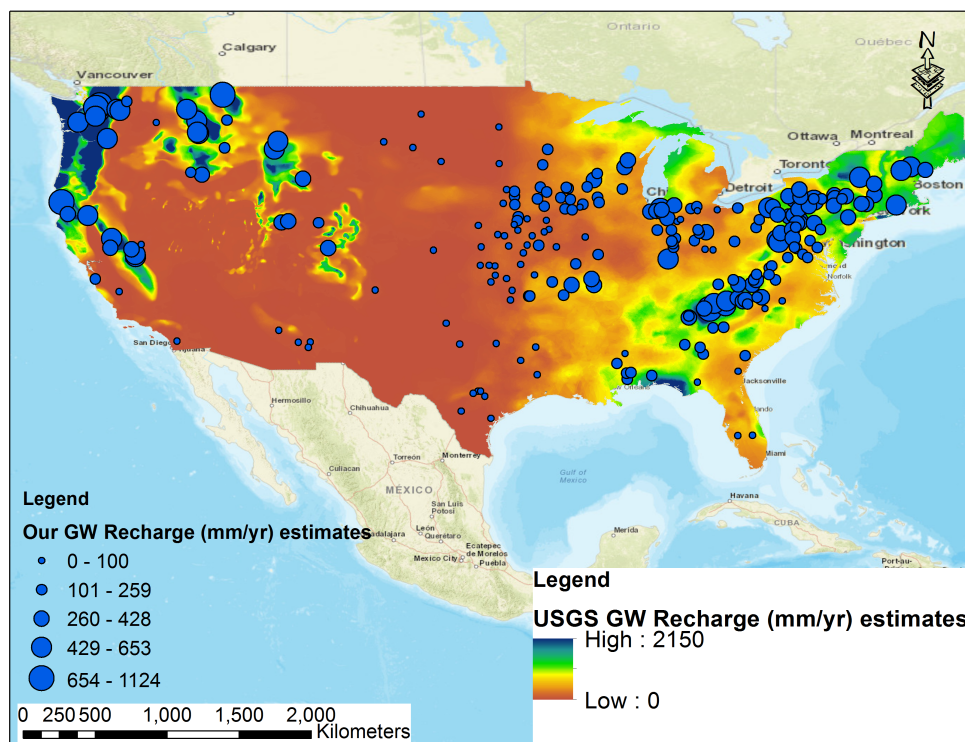
709

710 **Figure 9:** (A) Linear relationship between the Q_{50} flow of the FDC (a proxy of
711 average recharge rates at the catchment scale) and the mean baseflow estimated
712 from baseflow hydrographs. (B) Relationship between the Horton index and the Q_{50}
713 flow of the FDC for all catchments under study.

714



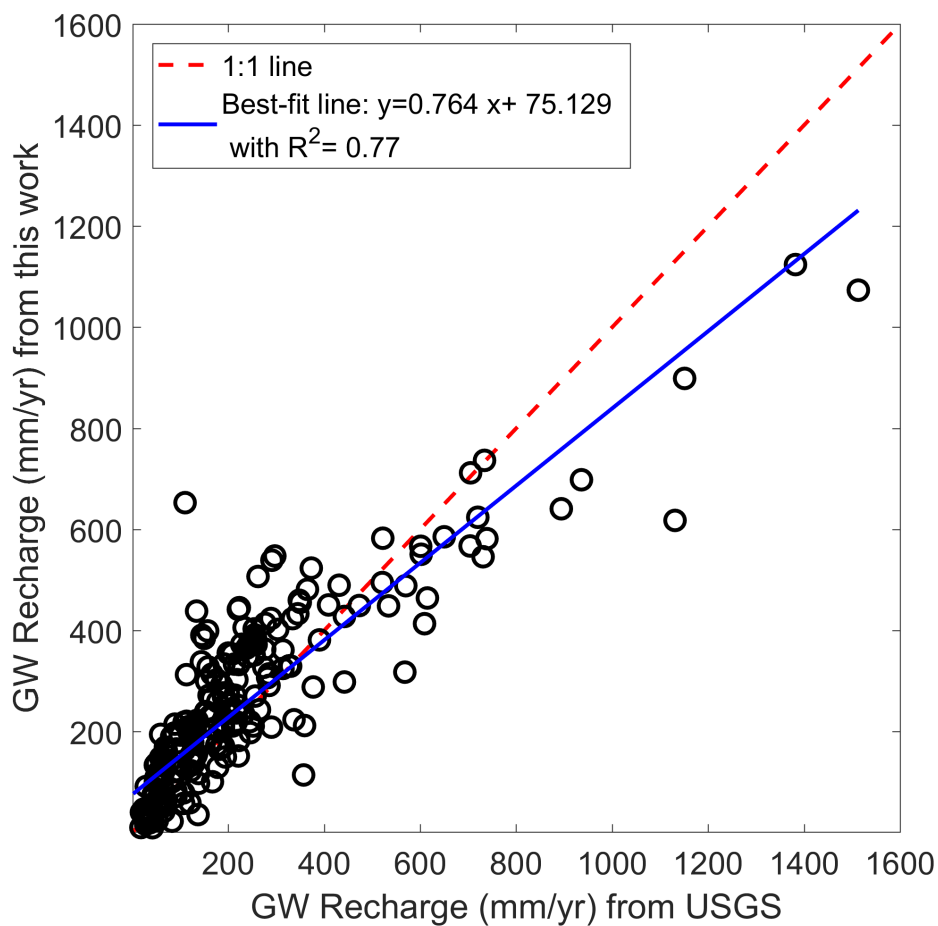
715



716

717 **Figure 10:** Horton Index-based estimates of average recharge rates (blue-markers)
718 overlain onto a USGS map [Wolock, 2003] of average recharge rates for the
719 conterminous US.

720



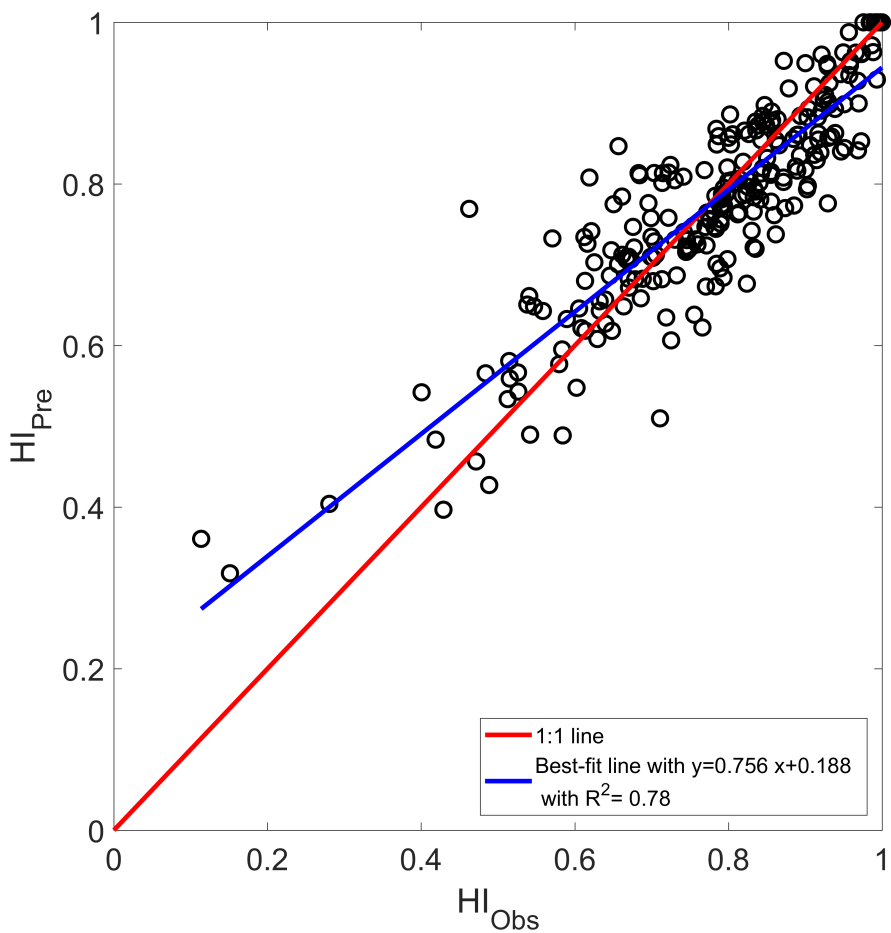
721

722 **Figure 11:** Inter-catchment comparison of HI based average recharge rates and

723 USGS-derived recharge rates (Wolock, 2003). The blue line is the regression line

724 through the data points and the red line is the 1:1 line.

725



726

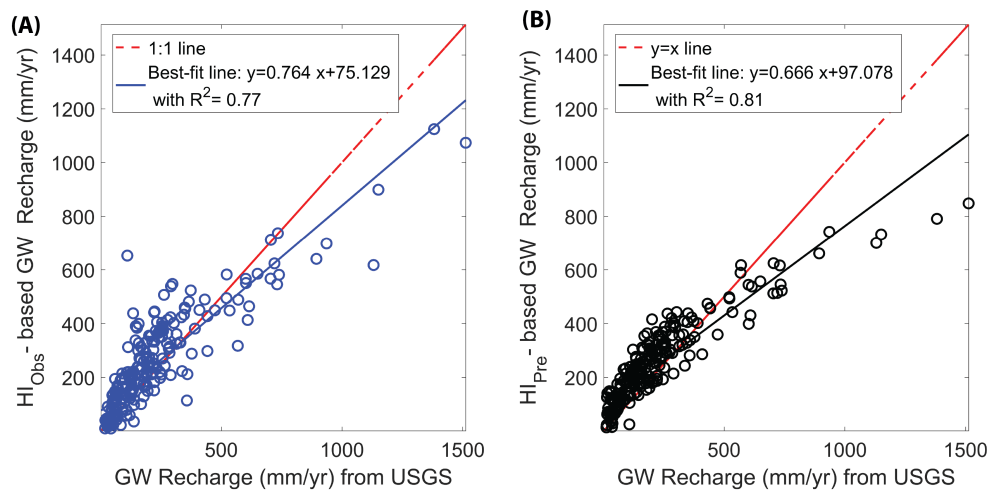
727 **Figure 12:** Comparison between predicted and observed HI using Equation (9). The

728 blue line is the best linear fit through the data points and the red line is the 1:1 line.

729



730



731

732 **Figure 13:** (A) Scatterplot between observed HI based groundwater recharge
733 (GWR) vs. USGS groundwater recharge with regression line (blue) and 1:1 line
734 (red); (B) scatterplot between predicted HI based GWR and USGS GWR with
735 regression line (black) and 1:1 line (red).

736

737

738



739 **Tables**

740 **Table 1:** Notation for Total and Deep Storage used in this Study

Description	Total storage	Deep storage
Storage	S_T	S_D
Storage at a given day t , $t = 1, 2, \dots, 365$	$S_T(t)$	$S_D(t)$
Maximum storage for a given year	S_T^{\max}	S_D^{\max}
Average maximum storage; N is number of years	$\bar{S}_T^{\max} = \frac{1}{N} \sum_{i=1}^{i=N} S_T^{\max}(i)$	$\bar{S}_D^{\max} = \frac{1}{N} \sum_{i=1}^{i=N} S_D^{\max}(i)$

741